



An attempt to improve cavitation erosion resistance of UHMWPE coatings through enhancing thermal conductivity via the incorporation of copper frames

Rui Yang^{a,b,c}, Xiuyong Chen^{a,c,d,*}, Ye Tian^a, Hao Chen^b, Nikolai Boshkov^e, Hua Li^{a,c,d}

^a Zhejiang Engineering Research Center for Biomedical Materials, Cixi Institute of Biomedical Engineering, Ningbo Institute of Materials Technology and Engineering, Chinese Academy of Sciences, Ningbo 315201, China

^b Department of Mechanical, Materials and Manufacturing Engineering, University of Nottingham Ningbo China, 199 Taikang East Road, Ningbo 315100, China

^c Key Laboratory of Marine Materials and Related Technologies, Zhejiang Key Laboratory of Marine Materials and Protective Technologies, Ningbo Institute of Materials Technology and Engineering, Chinese Academy of Sciences, Ningbo 315201, China

^d Center of Materials Science and Optoelectronics Engineering, University of Chinese Academy of Sciences, Beijing 100049, China

^e Institute of Physical Chemistry, Bulgarian Academy of Sciences, Sofia 1113, Bulgaria

ARTICLE INFO

Keywords:

Cavitation erosion
Composite coatings
Failure mechanism
In-situ observation
Thermal conductivity
UHMWPE

ABSTRACT

Ultrahigh molecular weight polyethylene (UHMWPE) coating and UHMWPE-copper (UHMWPE-Cu) coatings with different copper content were fabricated using a sintering method. The thermal conductivity of the coatings increased with the increasing copper content, but the resistance to cavitation erosion did not. The most optimised resistance was achieved by the coating with 8.3 wt% copper, whose thermal conductivity was 22.7% greater and total volume loss after 10 h cavitation erosion was 14% lower than those of pure UHMWPE coating. Underdosed and overdosed copper can significantly compromise the cavitation erosion resistance, as there is a trade-off between the benefit of enhancing thermal conductivity and the cost of weakening interface bonding. In addition, all the coatings exhibited the same damaged features. The in-situ observation was performed by a 3D profilometer to reveal the failure mechanism, finding that the process of the tilt-initiated peeling-off was the main source of the failure, which composed of preferential attack at the interface, tilting of the splats, and the detachment of the splat.

1. Introduction

Cavitation erosion is a common type of wear in hydrodynamic engineering, which causes severe damage on the components operated in fluid, such as blades of an impeller and a geometrically changed region of a pipeline [1]. The phenomenon of cavitation includes vaporisation, bubble generation, and bubble implosion, which results from a rapid decrease and subsequent increase in hydrodynamic pressure in a flowing liquid [2,3]. Upon the collapse of these cavitation bubbles, intense micro-jets are generated, releasing great kinetic and thermal energy and resulting in severe wear when impact to the surface of components [4,5].

Depositing protective coatings on the components subjected to cavitation erosion is one of the most effective anti-erosion strategies. Many studies have investigated the cavitation erosion behaviours of

metallic and metallic-ceramic based coatings, such as Fe-based coatings [6,7] and WC-based cermet coatings [8–10]. In the meanwhile, polymers usually employed as pore-sealers or binding agents which can enhance the cavitation erosion resistance of inorganic coatings. For example, introducing epoxy resin as a pore sealer to fill the pores and micro-cracks makes plasma sprayed ceramic coatings more resistant to cavitation erosion [11–13]. However, the studies focused on the cavitation erosion resistance performance of the polymer-based coatings are much fewer than those of the inorganic coatings.

According to the studies on polymer based coatings, both thermal sprayed nylon-epoxy resin and alumina reinforced epoxy resin had a lower cavitation erosion rate than that of 0.45% carbon steel [14]. Polyetheretherketone (PEEK) and polytetrafluoroethylene (PTFE) showed better cavitation erosion resistance compared with aluminium alloys [15]. The cavitation erosion resistance of glass fibre reinforced

* Corresponding author at: Zhejiang Engineering Research Center for Biomedical Materials, Cixi Institute of Biomedical Engineering, Ningbo Institute of Materials Technology and Engineering, Chinese Academy of Sciences, Ningbo 315201, China.

E-mail address: chenxiuyong@nimte.ac.cn (X. Chen).

<https://doi.org/10.1016/j.surfcoat.2021.127705>

Received 28 April 2021; Received in revised form 28 August 2021; Accepted 8 September 2021

Available online 15 September 2021

0257-8972/© 2021 Elsevier B.V. All rights reserved.

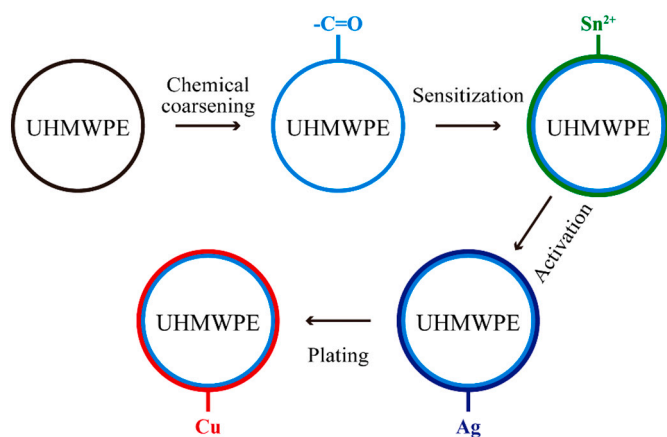


Fig. 1. Processing route of preparing the UHMWPE-Cu particles.

polymer (GFRP) composites, which was widely used for manufacturing of blades of propeller and impeller, can be further improved by optimising the fibre/epoxy distribution [16]. High-density polyethylene (HDPE) and ultrahigh molecular weight polyethylene (UHMWPE) showed outstanding cavitation erosion resistance in both ultrasonic vibratory apparatus (as per ASTM G32) [17,18] and rotating disk apparatus (as per ASTM G73) [19]. Apart from the excellent cavitation erosion resistance of polymer-based coatings, the studies also showed that local heating caused by the intense cavitating jets is an important fact in cavitation erosion of polymers [18], and the failure is due to synergetic effects between the locally imparted impulsive loads and heating of the material [20]. Thus, a possible method for further enhancing the erosion resistance of polymers can be improving the thermal conductivity to achieve better heat dissipation.

In this study, copper was introduced to sintered UHMWPE coatings, intending to improve the resistance to cavitation erosion by enhancing the thermal conductivity of the UHMWPE coatings. The UHMWPE and the UHMWPE-Cu coatings with different copper content were prepared on 316L stainless steel substrates using a sintering method, and their resistance to cavitation erosion was evaluated. Furthermore, the in-situ observation of the local damages was performed by 3D profilometer to help the understanding of the failure mechanism of the coatings.

2. Experimental procedure

2.1. Feedstock preparation

Commercially available UHMWPE powder (YUHWHA HIDDEN® U030 F, Korea Petrochemical, Korea) was used as the nascent feedstock, which has a molecular weight of 3 Mg/mol and a density of 0.93 g/cm³ according to the product specification. The powder was examined using a laser diffraction particle size analyser (S3500 special, Microtrac, USA) in ethanol fluid, measuring the average particle size of 125 μm and a size distribution ranged from 50 to 170 μm. The melting temperature of the UHMWPE powder is about 145 °C given by a differential scanning calorimeter (DSC, DSC 214, NETZSCH, Germany).

Table 1

Information of the UHMWPE and UHMWPE-Cu coatings fabricated in this work, where c_1 is the total mass of CuSO₄·5H₂O and c_2 is the total volume of the HCHO (37 wt%) added into the plating solution when preparing the feedstock, and ρ is the actual density of the coatings. The theoretical copper content of the coatings according to the amount of CuSO₄·5H₂O in the plating solution and the actual content according to the density measured are also given, as well as the Shore hardness (HD).

Materials	No.	c_1 , g	c_2 , mL	Theoretical Cu wt%	ρ , g/cm ³	Actual Cu wt%	Hardness, HD
UHMWPE	#00	–	–	–	0.925	0	71.3 ± 0.7
UHMWPE-Cu	#01	20	15	4.84	0.965	4.64	67.9 ± 0.9
UHMWPE-Cu	#02	40	30	9.24	0.999	8.30	67.8 ± 1.1
UHMWPE-Cu	#03	100	65	20.29	1.128	20.17	67.5 ± 1.1
UHMWPE-Cu	#04	200	125	33.73	1.280	31.08	68.5 ± 1.1

Multiple pre-treatments were implemented to electroless plate copper on UHMWPE, including chemical coarsening, sensitisation, and activation, of which the details can be found in the previous reports [21,22]. These pre-treatments can enhance the electroconductivity of the surface of UHMWPE particles to secure the success of the final electroless plating process. The processing route is demonstrated in Fig. 1. For a single batch, 100 g of the pre-treated UHMWPE powder was added into the plating solution at 55 °C for 1 h to prepare UHMWPE-Cu composite particles with core-shell structure. The original plating solution was composed of 20 g copper (II) sulfate pentahydrate (CuSO₄·5H₂O), 15 mL formaldehyde (HCHO, 37 wt%), 8 g sodium hydroxide (NaOH), and 24 g potassium sodium tartrate in 1 L deionised water. The chemicals that reacted during the plating process were CuSO₄·5H₂O, HCHO, and NaOH, as shown in Formula 1. The potassium sodium tartrate was used for stabilising copper ions and controlling the reaction speed. There were four batches of UHMWPE-Cu feedstocks prepared. Apart from the first batch, CuSO₄·5H₂O and HCHO were continuously added into the plating solution to prepare the feedstocks with different copper content. The total usage of the two chemicals for each batch was given in Table 1. During the plating process, the suspension was magnetically stirred, and its pH was carefully controlled around 11 by continuously dripping NaOH solution with a concentration of 0.01 mol/L during the plating process. All the chemicals used were GR grade (Sinopharm Chemical Reagent Ltd., China).



2.2. Coating preparation

The UHMWPE powder and the prepared UHMWPE-Cu powder were used to fabricate UHMWPE and UHMWPE-Cu coatings on 316L stainless steel substrates (316L SS, 20 mm in diameter, 10 mm in thickness). A sintering process was taken, as the high viscosity of the melt phase of UHMWPE prevents the implementation of other conventional methods. The schematic diagram of the apparatus is shown in Fig. 2(a).

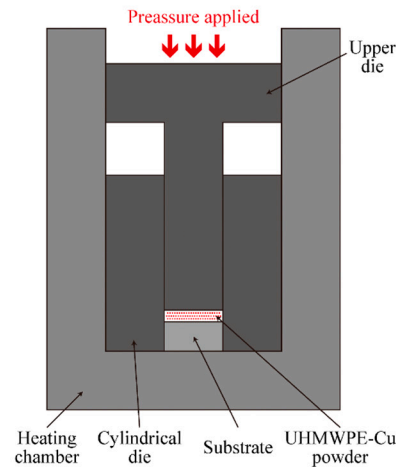
Prior to the sintering process, the top surface of each substrate was mechanically coarsened by sandblasting with 630–800 μm alumina particles then followed by ultrasonic cleaning in acetone bath and drying in warm air to achieve good adhesion between the substrate and the coatings. The bottom surface of the upper die was well polished before each sintering process to provide a smooth surface of the coating.

For each sintering process, 0.2 g powder was fed into the self-made sintering device and was pre-heated for 10 min at 80 °C with a pressure of 30 MPa to achieve better interface welding [23–25], which is crucial to minimise the porosity. Then the powder was heated for 45 min at 200 °C with a pressure of 20 MPa. This allows the consolidation of interfaces by chain diffusion across interfaces [23]. Finally, the sample was cooled to room temperature with a pressure of 20 MPa. It is previously reported that this cooling process can consolidate the interfaces by co-crystallisation [23,25–27].

2.3. Feedstock and coating characterisation

The feedstocks and the coatings were characterised by a scanning electron microscope (SEM, Quanta FEG 250, FEI, USA) operated at 5 kV,

a Sintering device



b Cavitation erosion test rig

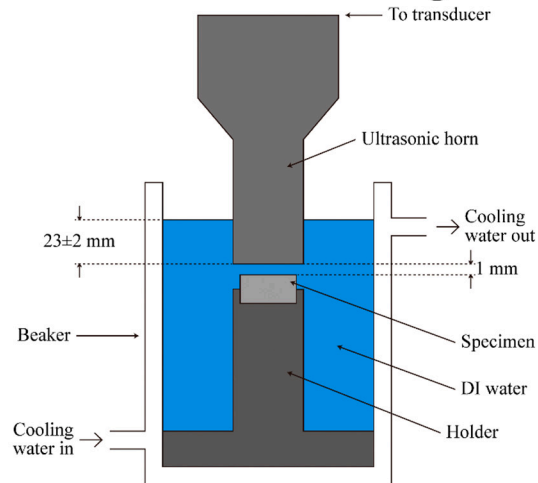


Fig. 2. Schematic diagrams of the sintering device (a) and the cavitation erosion test rig (b).

and the energy-dispersive x-ray spectrum (EDX) operated at 10 kV on the SEM. To investigate the cross section of particles and the coatings, the particles and the cut specimens were mounted in epoxy resin and then ground by 800, 1200, 2000, and 3000-grade SiC paper, respectively. The ground samples were further polished by a diamond suspension of 0.25 μm .

The density of the coatings was measured by the buoyancy method, and the thermal diffusivity was measured using light flash apparatus (LFA467, NETZSCH, Germany). The specific heat capacity of the coatings was given by DSC analysis. Thus, the thermal conductivity of the coatings can be calculated using the equation below [28], where λ is the coefficient of thermal conductivity, ρ is density, α is thermal diffusivity, and c_p is specific heat capacity.

$$\lambda = \rho\alpha c_p \quad (2)$$

The shore hardness (HD) of the coatings was measured by a type-D shore durometer (LX-D durometer, Chuanlu Measuring Tools Ltd., China). The usage of the powder for preparing each coating for hardness test was 1 g to give extra coating thickness, which ensured that the indenter would not penetrate the coating during the hardness test. The average hardness of each coating was acquired by measuring three samples, and there were five random points (the distance between each point was at least 5 mm) measured for each sample. The reading of the hardness value was taken at the 10th second during the indentation process for each measurement.

Tensile test (material testing machine 1 kN, ZwickLine Z1.0, ZwickRoell, Germany) was conducted at room temperature for the UHMWPE coating and the UHMWPE-Cu coating which exhibited the best resistance to cavitation erosion. The specimen for the tensile test was 12 mm in gauge length and 2 mm in width, and the crosshead speed is 10 mm/min. Young's modulus, ultimate tensile strength, maximum strain, and fracture energy were acquired based on the test result of three specimens for each coating.

2.4. Cavitation erosion test and in-situ observation

The cavitation erosion test of the as-received coated samples and polished 316L SS samples (by a pH-neutral colloidal silica suspension of 0.05 μm) was performed in deionised water using the indirect cavitation method. A typical ultrasound device (GBS-SCL 15K, GBSONIC, China) was utilised, and the parameters were in accordance with ASTM-G32 [29], where the output power was 2 kW, the output frequency was 20 kHz, and the peak-to-peak amplitude was 50 μm . A schematic diagram of the device is shown in Fig. 2(b). The tip of the vibrating horn was 23

± 2 mm below the liquid level. The separation distance between the surface of the specimen and the tip was set as 1 mm. The circulating water from the cooling system kept the temperature of the deionised water at 25 ± 1 °C. The specimens were subject to ultrasonic cavitation erosion for 10 h in total (12 h for the samples characterised by 3D profilometer). At every hour, the specimens were weighed on an electronic analytical scale. The resistance to cavitation erosion of the coatings is represented by the volume loss (V_{loss}), which were calculated as the equations given below, where m_{loss} is the mass loss of the test specimen and ρ is the density of the coating. The average volume loss of three samples was acquired for each type of coating.

$$V_{\text{loss}} = \frac{m_{\text{loss}}}{\rho} \quad (3)$$

The internal temperature of the coatings during cavitation erosion was also measured. The usage of the powder for preparing each coating for measuring internal temperature was 1 g to give extra coating thickness. A hole with a diameter of 0.25 mm and a depth of 10 mm was drilled by computer numerical control machine (5 axis machine, HUR-OCO, USA) on the side of the coating parallel to the surface, and the centre of the hole was 0.7 mm below the surface. A thermocouple (K-type, 0.13 mm wire diameter) was inserted into the hole and the internal temperature of the coating during cavitation erosion was measured by the thermocouple.

Apart from evaluating the volume loss and the internal temperature, the morphology of the coatings subjected to cavitation erosion for 10 h was observed in SEM operated at 5 kV. In addition, in-situ observation using the 3D profilometer (Up-Lambda 2, Rtec Instruments, USA) with a white light confocal lens was performed on the pure UHMWPE coating and the UHMWPE-Cu coating which exhibited the best resistance to cavitation erosion. The contour data of the coatings acquired by the 3D profilometer were further processed using MountainsMap® surface analysis software.

3. Results and discussion

3.1. Feedstock and coating characterisation

There were four batches of UHMWPE-Cu particles with different copper content prepared via electroless plating. Table 1 gives the information of the original UHMWPE and the prepared UHMWPE-Cu powders. The theoretical copper content was calculated based on the assumption that all the copper ions in the plating solution were transformed into the copper that enclosed the UHMWPE particles. The actual

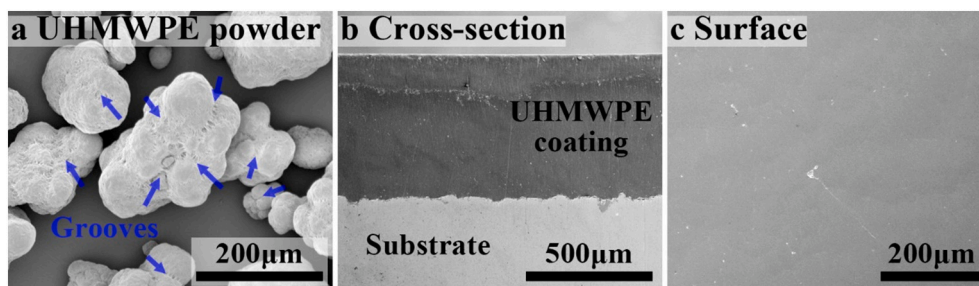


Fig. 3. SEM images of the original UHMWPE particles (a), the cross-section (b), and the surface (c) of the sintered UHMWPE coating. The ‘grooves’ at which sub-particles bonded together forming into large particles are highlighted by blue arrows.

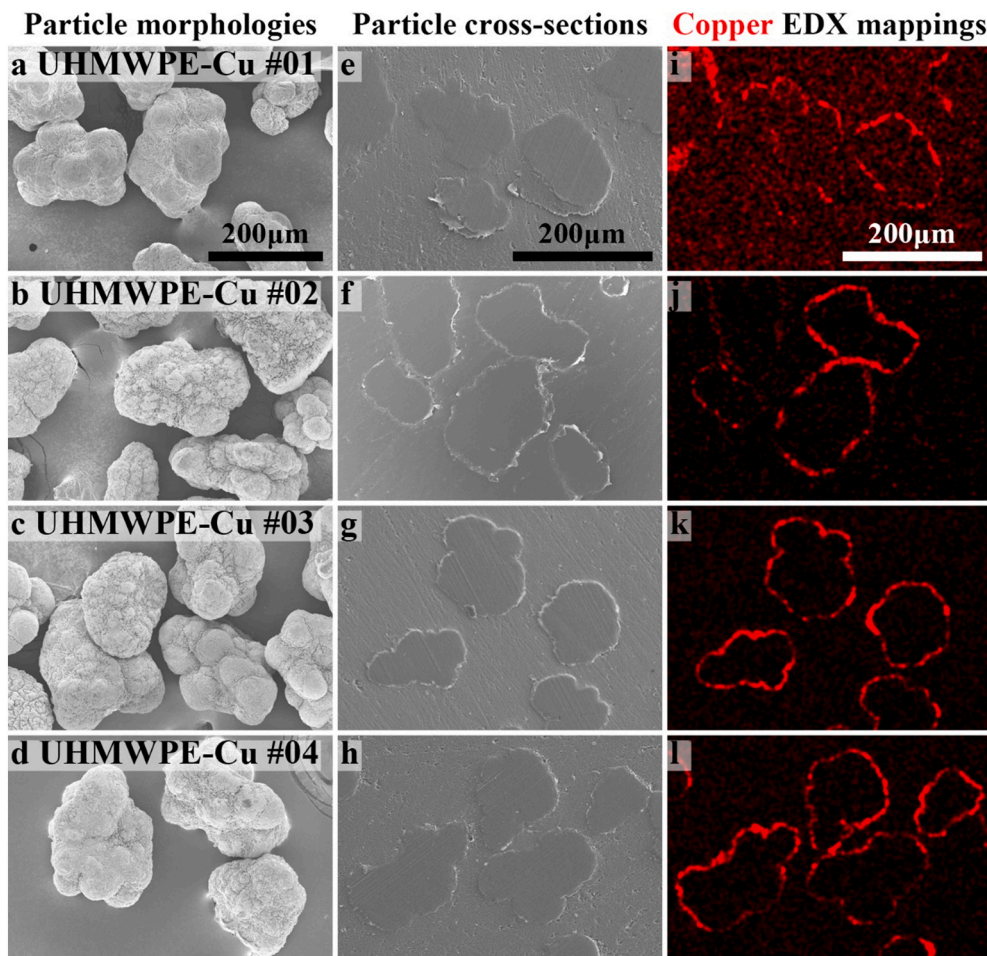


Fig. 4. SEM images of the UHMWPE-Cu particles: surface morphologies (a–d) and polished cross-sections (e–h) with the corresponding copper EDX mappings (i–l).

copper content was figured out according to the actual density of the coatings and assuming the density of the copper is 8.9 g/cm^3 . As given in Table 1, the value of actual copper content was quite close to the theoretical value, which shows that almost all the copper ions in the plating solution were transformed into copper and deposited to the polymer particles, indicating a good plating efficiency.

The surface morphology of the initial UHMWPE particles and the electroless plated UHMWPE-Cu particles are shown in Figs. 3(a) and 4 (a–d). The initial UHMWPE particles showed an ellipsoidal shape, and there were some ‘grooves’ (highlighted by blue arrows) with polymer fibrils that can be seen from each large particle, which indicates that a large particle may consist of some sub-particles. These ‘grooves’ were filled after electroless plating. To investigate how the polymer particles were enclosed by copper, EDX mapping Fig. 4(i–l) was conducted on the

cross section of the UHMWPE-Cu particles. As shown in Fig. 4(i), the UHMWPE-Cu #01 particles were partially enclosed by copper and the high image noise in the mapping result indicated a low content of copper, which is probably due to the insufficient copper ions in the plating solution failed to cover all the surface of the UHMWPE particles. As for the other batches of UHMWPE-Cu particles, the clear EDX mappings (Fig. 4(j–l)) evidenced the homogeneous distribution of copper and the core-shell structural feature.

The SEM images of the cross section of the UHMWPE and UHMWPE-Cu coatings are shown in Figs. 3(b) and 5(a–d). There was not any pore observed in both coatings. For the UHMWPE-Cu coatings, the interface among the splats became clearer as the copper content increased. Also, the EDX mappings (Fig. 5(e–h)) showed that a ‘copper frame’ was successfully formed inside the polymer. The surface morphology of the

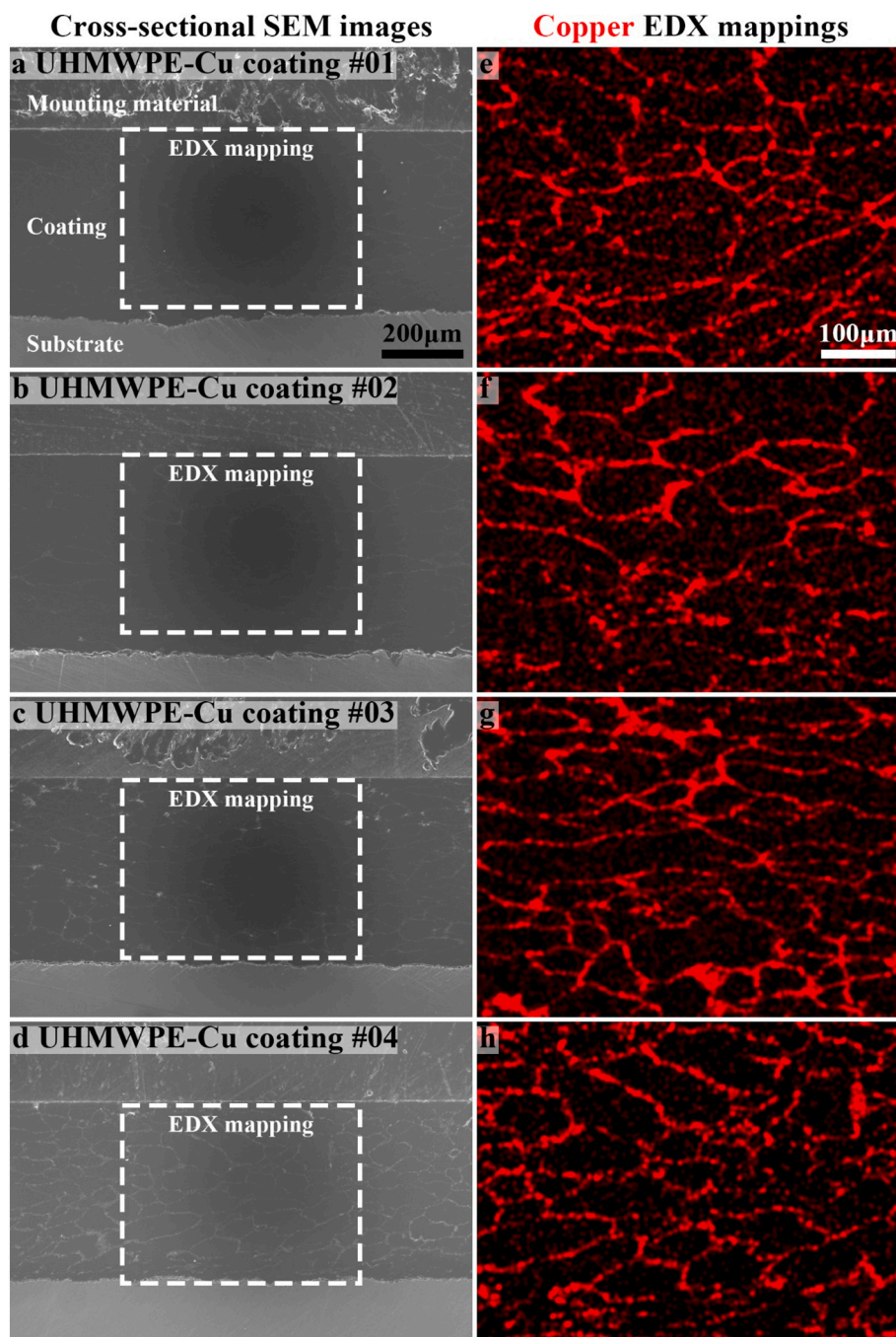


Fig. 5. SEM images of the cross-section of the UHMWPE-Cu coatings (a–d) and the corresponding copper EDX mapping (e–h).

UHMWPE and UHMWPE-Cu coatings are shown in Figs. 3(c) and 6(a–d). All the coatings exhibited a smooth and almost defect-free surface. For the surface of the UHMWPE-Cu coating, some areas were not covered with copper according to the copper EDX mapping (Fig. 6(e–h)). There are two possible reasons for this. Firstly, some UHMWPE particles were only partially enwrapped with copper during the electroless plating. Secondly, some copper was peeled off when separating the sample from the upper die, as the bonding between copper and the upper die (which was made from stainless steel) was greater than that between copper and polymers.

The physical properties of the coatings related to thermal conductivity were tabulated in Table 2. As expected, pure UHMWPE coating exhibited the lowest thermal conductivity and the thermal conductivity of the UHMWPE-Cu coatings increased with the increasing copper

content. The internal temperature of the coatings being subjected to cavitation erosion was tabulated in Table 3, which evidenced that improving thermal conductivity can effectively reduce the internal temperature. The enhanced thermal conductivity may benefit the cavitation erosion resistance, as local heating is one of the concerns for the polymers subjected to cavitation erosion [18,20]. However, there is a risk that the addition of copper would reduce the strength of interface bonding among the splats, because the bonding of UHMWPE-copper is weaker than the bonding of pure UHMWPE. As shown in the Shore hardness (HD) of the coatings in Table 1, the hardness of the pure UHMWPE coating was 71.3 HD, while the hardness of the UHMWPE-Cu coatings was slightly lower, which was about 68 HD. The reduced hardness could be attributed to the weak interface bonding between UHMWPE and copper. Weak interface bonding could reduce the

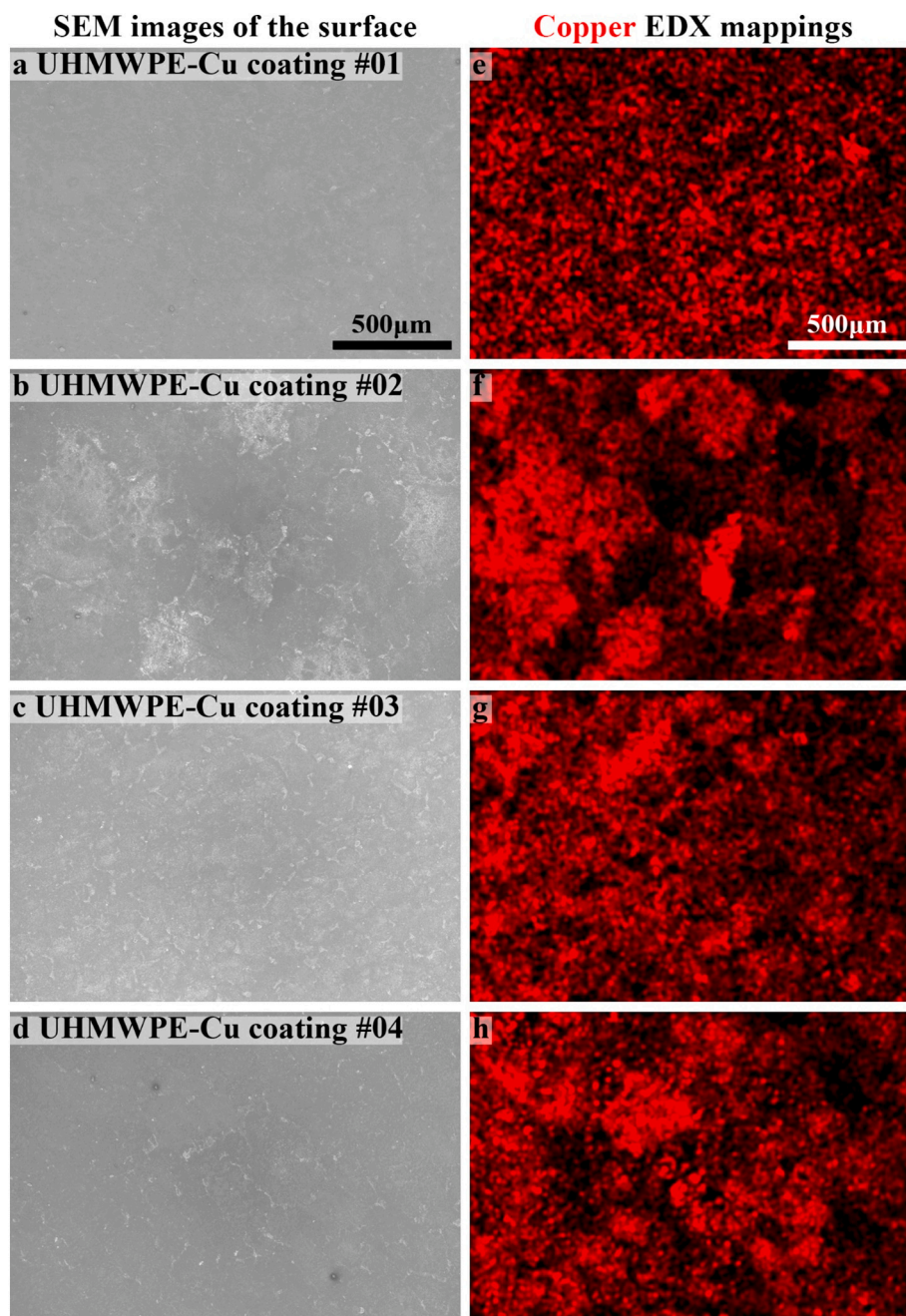


Fig. 6. SEM images of the surface of the UHMWPE-Cu coatings (a–d) and the corresponding copper EDX mapping (e–h).

resistance to cavitation erosion as numerous studies showed that cavitation erosion preferentially attacks at the interfaces of the splats [5]. In addition, decreasing in hardness is recognised to be harmful to the cavitation erosion resistance. Thus, the ability of UHMWPE-Cu coating to resist cavitation erosion could be compromised if the mechanical properties are considered solely.

3.2. Cavitation erosion test

The resistance to cavitation erosion of these coatings was quite different according to the volume loss. The total volume losses of the UHMWPE coating, the UHMWPE-Cu coatings, and bulk 316L stainless steel after 10 h exposure to cavitation erosion in deionised water were tabulated in Table 4. In the meanwhile, the plots of the cumulative volume loss are displayed in Fig. 7. As the difference in the cumulative

volume loss of the samples was so huge that the curves of the volume loss could not be put in a single graph. The curves of the UHMWPE coating, the UHMWPE-Cu #02 coating, and the 316L stainless steel were plotted in Fig. 7(a) and the curves of the other UHMWPE-Cu coating were plotted in Fig. 7(b). According to the table and the figure, the lowest total volume loss among the coatings was achieved by the UHMWPE-Cu #02 coating with a copper content of 8.30 wt%, which was 14% lower than that of pure UHMWPE coating and was close to that of bulk 316L stainless steel. Furthermore, according to Fig. 7(a), the cumulative volume loss of the UHMWPE-Cu #02 coating was less than that of the pure UHMWPE coating through the whole test, indicating that introducing copper network to the UHMWPE coating was able to improve the resistance to cavitation erosion. However, underdosed or overdosed copper in the UHMWPE coating can significantly compromise the resistance to cavitation erosion. As shown in Table 4 and Fig. 7, the total

Table 2

Physical properties of the UHMWPE and UHMWPE-Cu coatings related to thermal conductivity, where ρ is density, α is thermal diffusivity, c_p is specific heat capacity, and λ is the coefficient thermal conductivity calculated according to ρ , α and c_p . The improvement of thermal conductivity in percentage compared with the pure polymer coating, $\Delta\lambda\%$, is also given.

Coatings	No.	ρ , g/cm ³	α , mm ² /s	c_p , J/(kg·K)	λ , W/(m·K)	$\Delta\lambda\%$, %
UHMWPE	#00	0.925	0.225	2097	0.436	–
UHMWPE-Cu	#01	0.965	0.237	2033	0.465	6.7
UHMWPE-Cu	#02	0.999	0.270	1983	0.535	22.7
UHMWPE-Cu	#03	1.128	0.297	1757	0.588	34.9
UHMWPE-Cu	#04	1.280	0.395	1634	0.826	89.4

Table 3

The internal temperature of the UHMWPE and the UHMWPE-Cu coatings when subjected to cavitation erosion.

Coatings	PE #00	PE-Cu #01	PE-Cu #02	PE-Cu #03	PE-Cu #04
Temperature	46.86 ± 0.33	35.15 ± 0.05	32.6 ± 0.07	31.65 ± 0.11	26.80 ± 0.07

Table 4

The total volume losses of the UHMWPE coating, the UHMWPE-Cu coatings, and bulk 316L stainless steel after 10 h exposure to cavitation erosion.

Samples	Volume loss, mm ³
UHMWPE coating #00	4.32 ± 0.46
UHMWPE-Cu coating #01	30.63 ± 5.41
UHMWPE-Cu coating #02	3.80 ± 0.43
UHMWPE-Cu coating #03	50.88 ± 12.58
UHMWPE-Cu coating #04	66.09 ± 7.99
Bulk 316L stainless steel	3.90 ± 0.69

volume loss of the UHMWPE-Cu #01, #03, and #04 coatings was much greater than that of the UHMWPE-Cu #02 coating by approximately one order of magnitude.

The SEM images of the as-received coatings and the coatings subjected to cavitation erosion for 10 h are shown in Fig. 8. Surprisingly, despite of having different copper content and huge differences in volume loss, the UHMWPE coating and all the UHMWPE-Cu coatings had

the same damaged features, which were tilted piece (pointed by blue arrow), flat basin (enclosed by blue square), and rough cavitation pit (enclosed by red circle). The magnified SEM images of these damaged features were also displayed in Fig. 9. In addition, all the coatings exhibited ductile ruptures suggesting a plastic deformation, while there were fibrils observed on the surface and the wall of large cavitation pits (Fig. 9(k-o)) indicating local heating and possibly partially melting, which is also reported in the other study [19]. The interfaces between the splats and the interfaces (the ‘grooves’ in Fig. 3(a)) between the sub-particles are the sites where interparticle failure is most likely to take place, which is also frequently occurred to the UHMWPE processed by high velocity compaction [30]. Thus, the continuous strikes at these interfaces may initiate the tilt of the polymer piece (Fig. 9(a-e)). Further exposure to cavitation erosion may cause the piece even more tilted. Then, a rupture was occurred, separating the tilted piece from the surface, and leaving a basin at the site (Fig. 9(f-j)). As the area beneath the tilted piece was almost free of the impact of cavitation bubble until the piece is torn off, the surface at the bottom of the basin was less damaged than the other area. The large rough pits in Fig. 9(k-o) may be sourced from the basin which further took the damage from cavitation erosion. It is worth noticing that the surface of these large pits was much rougher than that of the other area, while the fibrils at these large pits were also much denser. These indicate that the edge of the pits took more damage from the local heating, possibly due to low heat dissipation [20].

3.3. In-situ observation and failure mechanism

According to the damaged features presented before, it is suspected that a basic failure mechanism is tilt-initiated peeling-off of the materials. Thus, in-situ observation of the cavitation erosion process is necessary to help the understanding of the mechanism. As there must be changes in the local altitude of the splat if the splat was tilted during the cavitation erosion, surface profilometer was used for monitoring the altitude change of a surface. In addition, surface roughness or surface profile can also be applied for evaluating the damage caused by cavitation erosion [16,19,31]. The in-situ surface profile observation was performed on the UHMWPE #00 and the UHMWPE-Cu #02 coatings.

Figs. 10 and 11 show the profile of the surface of the UHMWPE #00 and the UHMWPE-Cu #02 coatings after various periods of exposure to cavitation erosion. Despite having a rougher surface at the beginning, the ultimate surface roughness of the UHMWPE-Cu #02 coating, which exhibited the lowest volume loss during cavitation erosion compared with the others, was less than that of pure UHMWPE coating. The higher initial surface roughness of the UHMWPE-Cu #02 was possibly attributed to the coarse nature of the copper shells and the peeling-off of the copper when separating the coating from the upper die. The highlighted

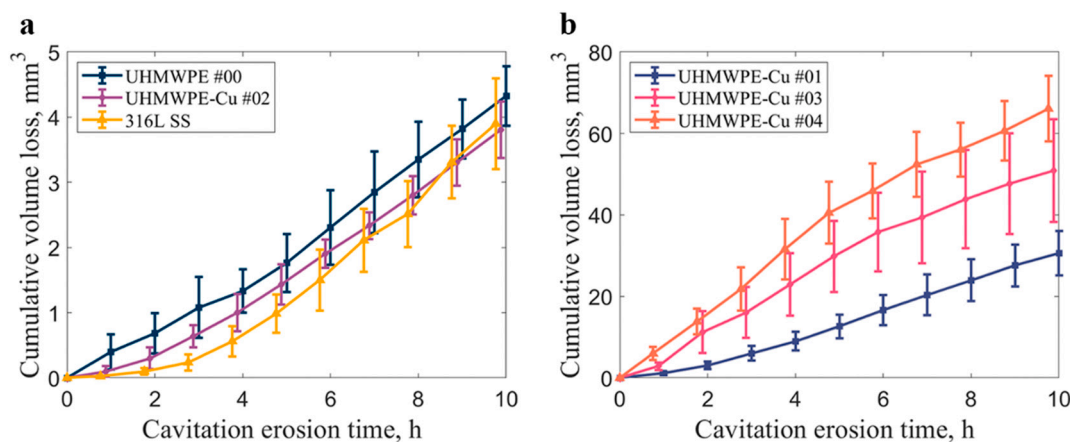


Fig. 7. Plots of the cumulative volume loss of the samples subjected to cavitation erosion in dionised water for 10 h: UHMWPE coating #00, UHMWPE-Cu coating #02, and 316L stainless steel in figure (a); UHMWPE-Cu coatings #01, #03, and #04 in figure (b).

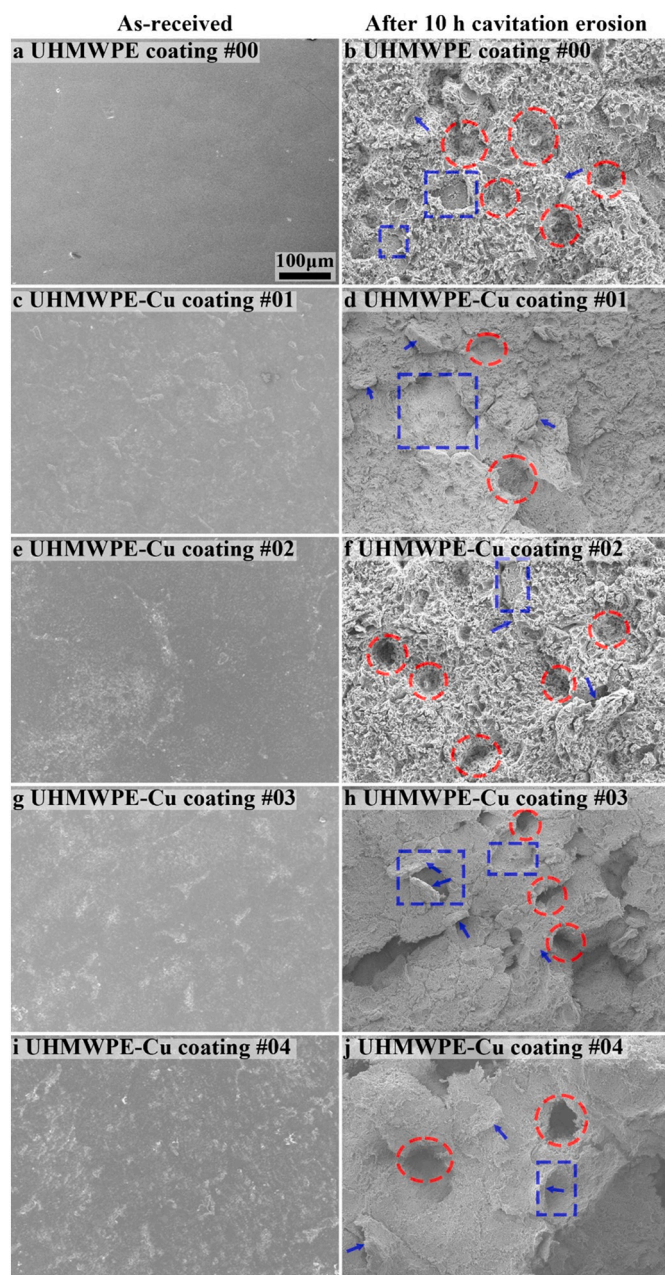


Fig. 8. SEM images of the surface of the as-received UHMWPE and UHMWPE-Cu coatings (left column) and the surface of the coatings after 10 h cavitation erosion (right column) with the damaged features highlighted: Tilted piece (pointed by blue arrow), basin (enclosed by blue square), and rough cavitation pit (enclosed by red circle).

regions in Figs. 10 and 11 show that some sites with abrupt high altitudes started to appear at the early stage of cavitation erosion. Then, after further cavitation erosion, these sites usually left pits with great depressions on the surface. These pits could either wear gradually or get extended to the site where a neighbour splat is subjected to the peeling-off which leads to another sudden detachment of the splat. Thus, the tilt-initiated peeling-off not only existed at the early stage of cavitation erosion but continuously occurred during the whole process of cavitation erosion, which caused significant damage to the coatings.

The failure mechanism of the coatings subjected to cavitation erosion is revealed based on the in-situ surface profile observations (Figs. 10, 11) and the previous SEM images (Figs. 8, 9), which is the same for all the coatings. Fig. 12 shows a schematic diagram that demonstrates the

failure mechanism. At the early stage of cavitation erosion, the implosion of cavitation bubbles makes the surface rough and preferentially attacks at the interfaces between the splats (Fig. 12(a–b)). As more strikes at the interfaces and some vulnerable spots of the splat, the splat starts to tilt (Fig. 12(b–c)). When the vulnerable spot finally gets penetrated and ruptured, the tilted part of the splat is worn off, leaving a large pit on the surface (Fig. 12(c–d)). Finally, further attacks at the interface of the rest part of the splat result in the tilting and peeling-off of the part of the splat, and the pit expands.

3.4. The role of copper

To investigate the effect of copper addition on the mechanical properties of UHMWPE coatings, tensile test was performed on the pure UHMWPE and the UHMWPE-Cu #02 specimens. According to the results (Fig. 13 and Table 5), apart from a slight decrease in Young's modulus, ultimate tensile strength, maximum strain, and fracture energy of UHMWPE were significantly compromised when copper was introduced. Furthermore, the SEM images of the fractured specimens (Fig. 13(b–c)) indicated the poor internal bonding of the internal bonding of the UHMWPE-Cu, which also explained the UHMWPE-Cu failed more quickly than the pure UHMWPE during tensile test. Thus, it is expected that the cavitation erosion resistance of the UHMWPE-Cu coating would have been compromised. However, the cavitation erosion resistance of the UHMWPE-Cu #02 coating was improved. This indicates that there is another variable affecting the cavitation erosion resistance of UHMWPE, apart from mechanical properties and internal bonding. According to Table 3, the internal temperature of all the coatings during cavitation erosion is increased from the temperature of test medium (25 °C) up to 47 °C, and the increment of internal temperature of the UHMWPE-Cu #02 coating was 14 °C lower than that of pure UHMWPE coating. Studies are reporting that higher mechanical stability with respect to temperature may provide better cavitation erosion resistance [19,32] and suggesting a significant increase in the local temperature up to the melting point of the UHMWPE with relatively lower molecular weight may cause the disentanglement of the polymer at the site resulting in significant damage [19]. In addition, other studies on the erosion and heating of polyurea under cavitating jets show a strong correlation between the temperature rise and material failure [20,33,34]. Thus, the improved cavitation erosion resistance of the UHMWPE-Cu #02 coating could be attributed to its lower internal temperature increment compared to the pure UHMWPE coating, resulting in a lower reduction of mechanical properties, and further providing better resistance to cavitation erosion. The reduction of the internal temperature increment could be further attributed to the enhanced thermal conductivity due to the addition of copper.

Based on the suggestion that the enhanced thermal conductivity may improve the cavitation erosion resistance, despite having compromised mechanical properties, the other UHMWPE-Cu coatings could have been more resistant to cavitation erosion. However, the UHMWPE-Cu #01, #03, and #04 coatings exhibited very poor cavitation erosion resistance. Therefore, possible suggestions are proposed: On the one hand, as the interface of the splats is preferentially attacked by cavitation erosion, when the copper is underdosed, instead of mitigating the cavitation erosion, the site of the copper could probably be a defect which might speed up the propagation of damage at the interface and accelerate the tilting of the splat for the poor bonding to the UHMWPE. Furthermore, insufficient copper means the copper network inside the polymer may not be continuous and the route of heat dissipation is blocked. On the other hand, as the interface of copper and UHMWPE is weaker than that of pure UHMWPE, despite of enhanced thermal conductivity, overdosed copper might significantly reduce the bonding strength at the interface, resulting in poor resistance to cavitation erosion.

Thus, the amount of copper should be controlled carefully as both underdosing and overdosing of copper can significantly compromise the cavitation erosion resistance of the UHMWPE-Cu coating. In addition,

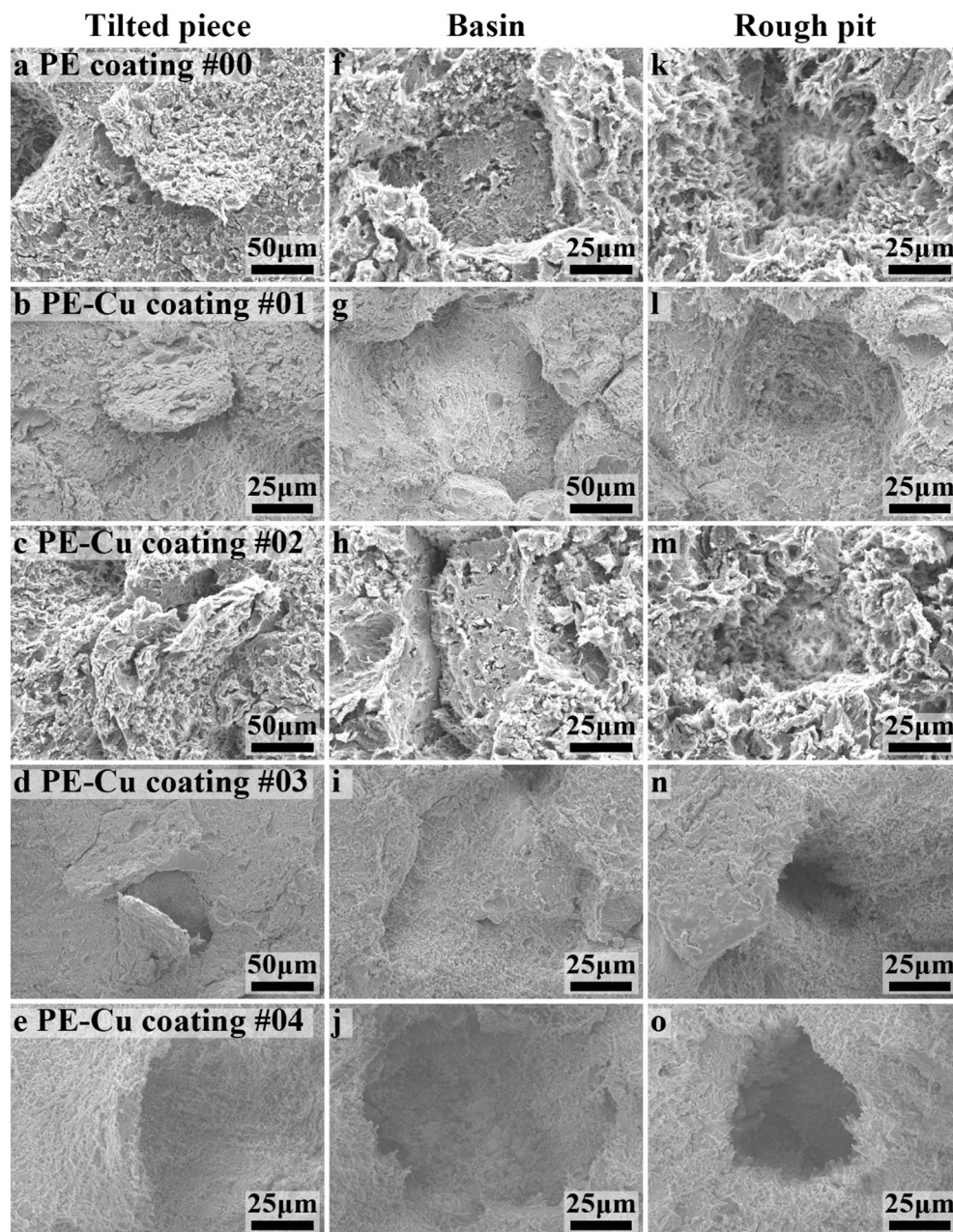


Fig. 9. SEM images of the surface of UHMWPE (the first row) and the UHMWPE-Cu (the rest of rows) coatings after 10 h cavitation erosion showing different features of damage: tilted piece (a–e), flat basin (f–j), and rough cavitation pit (k–o).

the investment of copper to affect the resistance to cavitation erosion of the UHMWPE coating may be an inverse U-shaped curve, which means there is probably a most optimised point that the subtraction of the benefit of enhancing thermal conductivity and the cost of weakening interface bonding gives the greatest resistance to cavitation erosion.

4. Conclusions

(1) The present study improved the cavitation erosion resistance of UHMWPE coatings by introducing copper to the coatings. A processing route for fabricating UHMWPE-Cu powder and the coating was proposed. All the sintered UHMWPE-Cu coatings with different copper content had a homogenous dense microstructure and a copper 'frame' between the UHMWPE splats. The thermal conductivity of the coating has a positive correlation with the amount of copper in the coating.

- (2) The increment of the internal temperature of the UHMWPE-Cu coatings was much less than that of pure UHMWPE coating during cavitation erosion, indicating the heat energy from the impact sites may dissipate more quickly at the UHMWPE-Cu coatings than at the pure UHMWPE coating, which is possibly attributed to the enhanced thermal conductivity from the addition of copper.
- (3) There is a trade-off between the benefit of enhancing thermal conductivity and the cost of weakening interface. Overdosed and underdosed copper can significantly reduce the resistance to cavitation erosion. The most optimised resistance was achieved by the coating with 8.3 wt% copper, whose thermal conductivity was 22.7% greater and total volume loss after 10 h cavitation erosion was 14% lower than those of pure UHMWPE coating.
- (4) All the coatings exhibited the same damaged features. The in-situ observation using a 3D profilometer was conducted to investigate

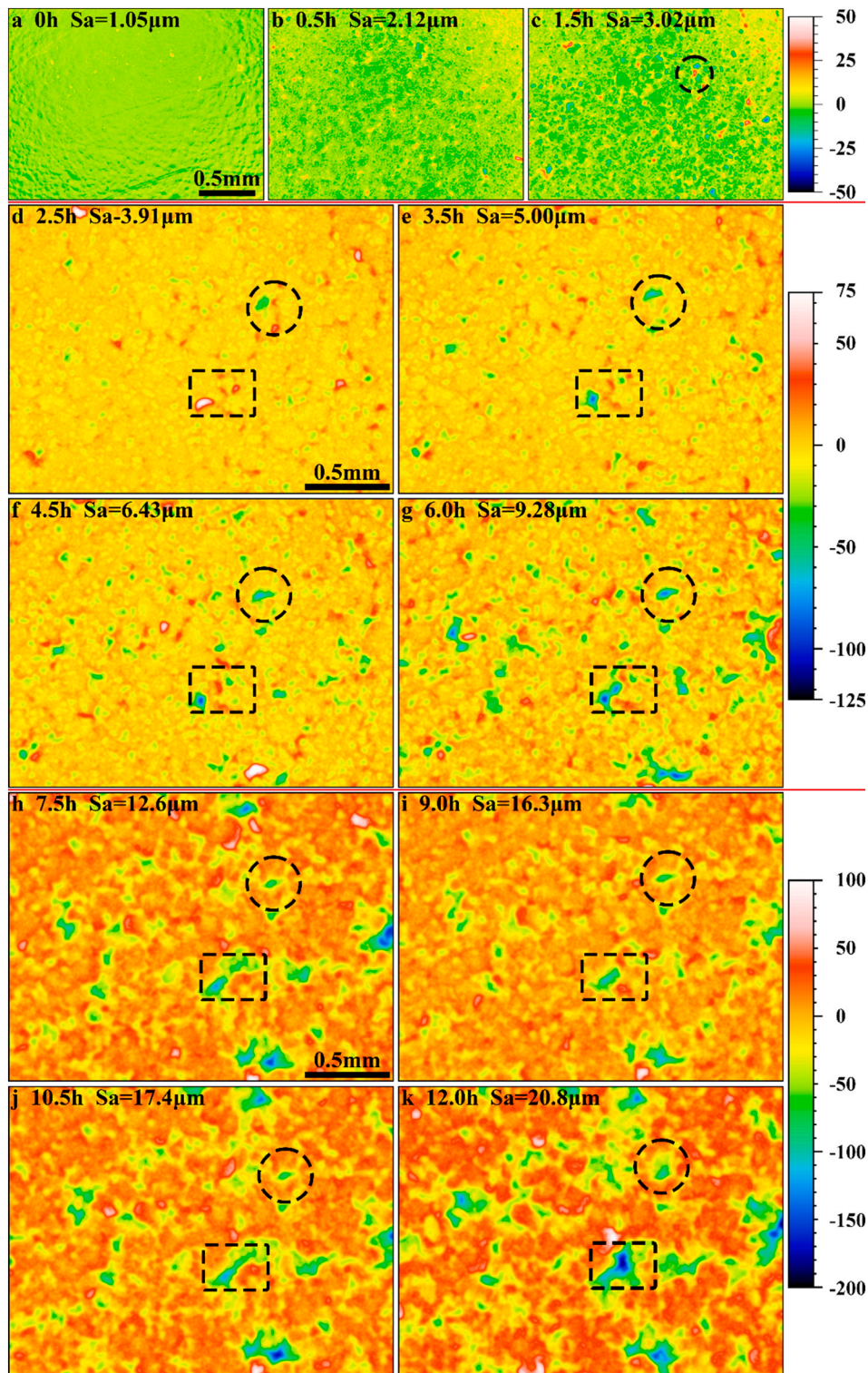


Fig. 10. The profile of the surface of the UHMWPE #00 coating after various periods of exposure to cavitation erosion (labelled in headline) at the same observation point, where two regions are highlighted which further evidence the peeling-off and the rupture of tilted matter pieces.

the cavitation erosion behaviour of the coatings. The tilt-induced peeling-off of the materials contributed to the most of wear. The failure mechanism, which is composed of preferential attack at the interface, tilting of the splats, and the detachment of the splat, is concluded to demonstrate the cavitation erosion behaviour of the coatings, which may provide the understanding of the behaviour of other similar materials.

CRediT authorship contribution statement

Rui Yang: Methodology, Investigation, Writing - Original Draft, Software.
 Xiuyong Chen: Conceptualization, Writing - Review & Editing, Supervision.
 Ye Tian: Methodology, Investigation.

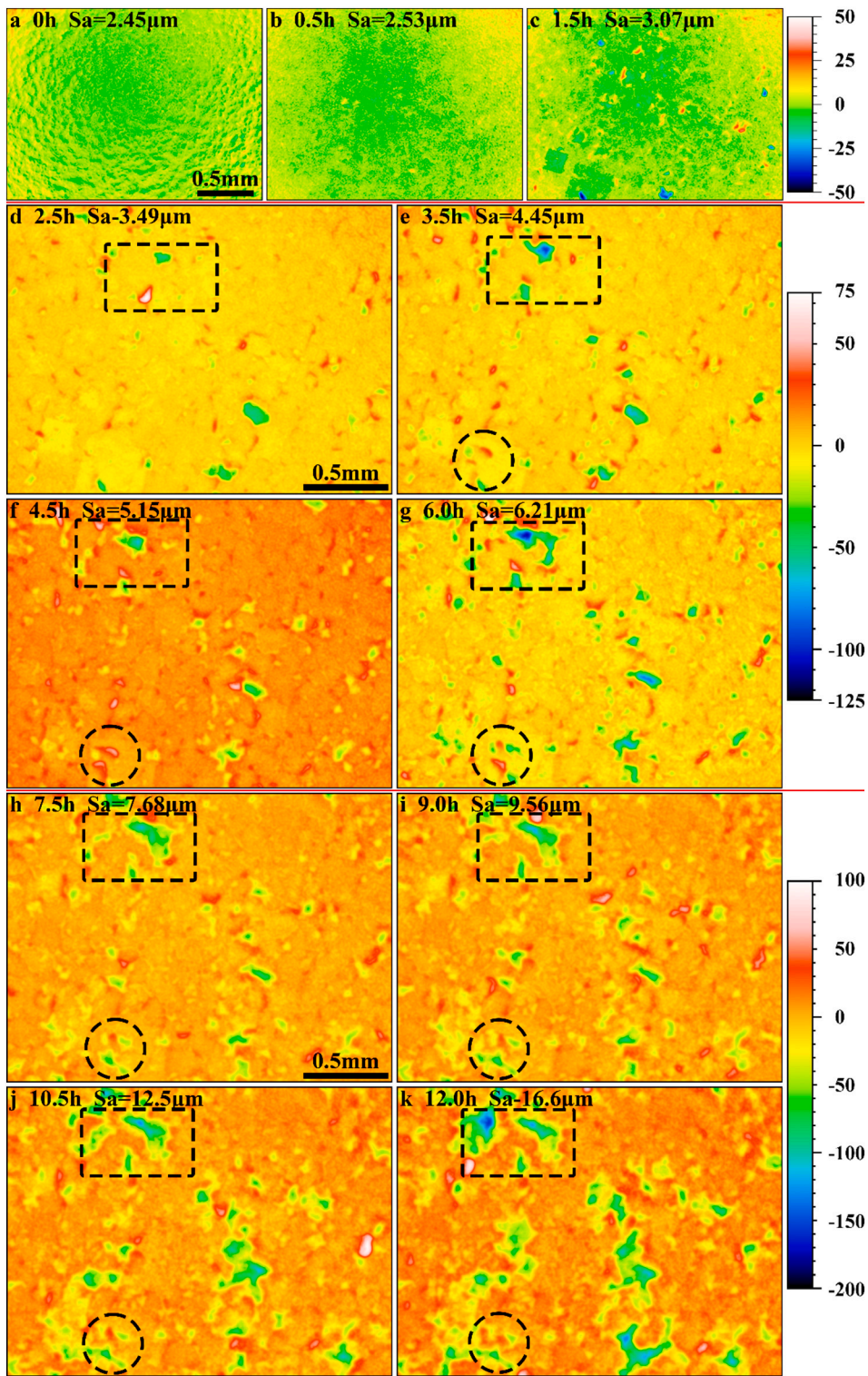


Fig. 11. The profile of the surface of the UHMWPE-Cu #02 coating after various periods of exposure to cavitation erosion (labelled in headline) at the same observation point, where two regions are highlighted which further evidence the peeling-off and the rupture of tilted matter pieces.

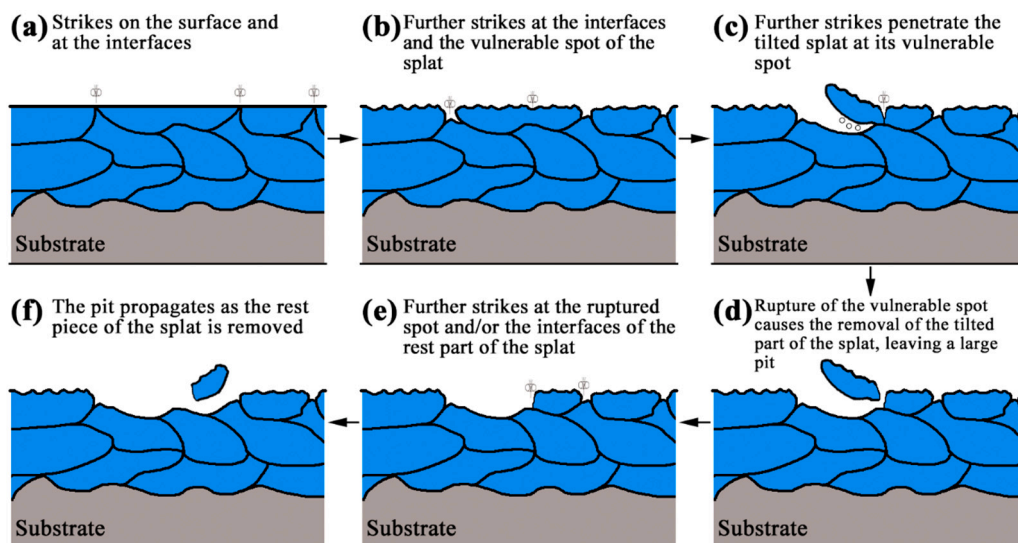


Fig. 12. Schematic diagram the failure mechanism of the coatings subjected to cavitation erosion.

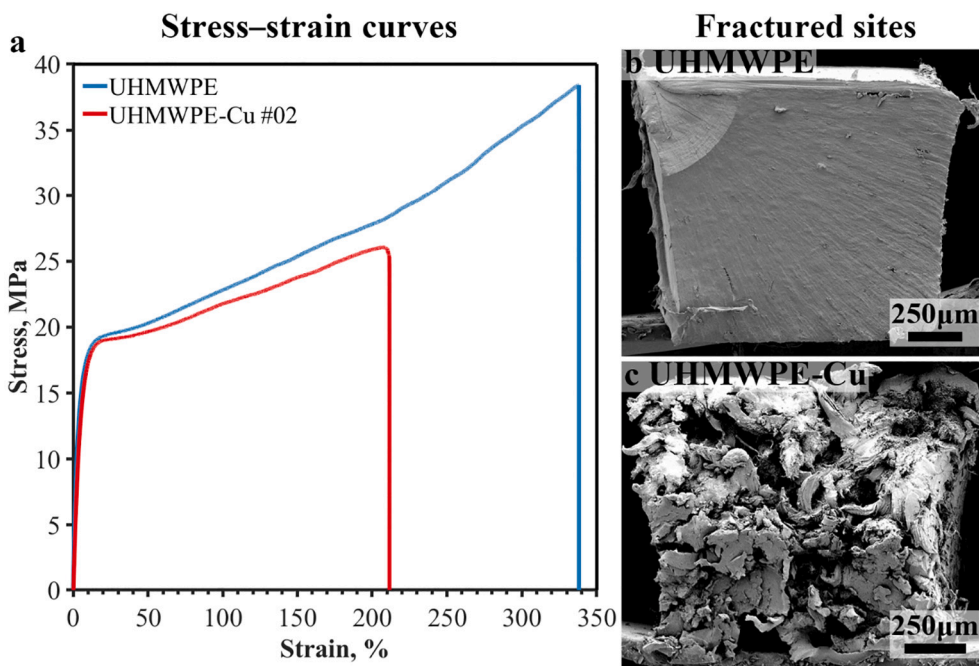


Fig. 13. Stress-strain curves of the UHMWPE and the UHMWPE-Cu#02 (a) at room temperature and SEM images of the fractured sites (b-c).

Table 5

Mechanical properties of the UHMWPE and the UHMWPE-Cu specimens evaluated by tensile test at room temperature, where E is Young's modulus, σ_m is ultimate tensile strength, ϵ_m is maximum strain, and G_f is fracture energy.

Specimens	E, MPa	σ_m , MPa	ϵ_m , %	G_f , MJ/m ³
UHMWPE	647 ± 38	37.9 ± 0.5	335 ± 5	48.5 ± 2.5
UHMWPE-Cu #02	596 ± 78	26.7 ± 1.2	226 ± 14	19.9 ± 2.4

Hao Chen: Review & Editing.
 Nikolai Boshkove: Review & Editing.
 Hua Li: Review & Editing.

Declaration of competing interest

The authors declare that they have no known competing financial interests or personal relationships that could have appeared to influence the work reported in this paper.

Acknowledgements

This study was supported by the Chinese Academy of Sciences President's International Fellowship Initiative (grant # 2020VEA0005), National Natural Science Foundation of China (grant # 21705158 and 51901107), Ningbo Natural Science Foundation Programme (grant # 2019A610176), and National Key Lab Fund (grant # JCKY61420052013).

References

- [1] P. Kumar, R.P. Saini, Study of cavitation in hydro turbines—a review, renew, Sustain. Energy Rev. 14 (2010) 374–383, <https://doi.org/10.1016/j.rser.2009.07.024>.
- [2] J. Franc, J. Michel, Introduction the main features of cavitating flows, in: Fundam. Cavitation, Kluwer Academic Publishers, Dordrecht, 2005, pp. 1–14, https://doi.org/10.1007/1-4020-2233-6_1.
- [3] C.E. Brennen, Cavitation and Bubble Dynamics, Cambridge University Press, Cambridge, 2013, <https://doi.org/10.1017/CBO9781107338760>.
- [4] B.K. Sreedhar, S.K. Albert, A.B. Pandit, Cavitation damage: theory and measurements - a review, Wear. 372–373 (2017) 177–196, <https://doi.org/10.1016/j.wear.2016.12.009>.
- [5] S. Lavigne, F. Pougoum, S. Savoie, L. Martinu, J.E. Klemberg-Sapieha, R. Schulz, Cavitation erosion behavior of HVOF CaviTec coatings, Wear. 386–387 (2017) 90–98, <https://doi.org/10.1016/j.wear.2017.06.003>.
- [6] L. Qiao, Y. Wu, S. Hong, J. Cheng, Ultrasonic cavitation erosion mechanism and mathematical model of HVOF sprayed Fe-based amorphous/nanocrystalline coatings, Ultrason. Sonochem. 52 (2019) 142–149, <https://doi.org/10.1016/j.ulsonch.2018.11.010>.
- [7] L. Qiao, Y. Wu, S. Hong, J. Zhang, W. Shi, Y. Zheng, Relationships between spray parameters, microstructures and ultrasonic cavitation erosion behavior of HVOF sprayed Fe-based amorphous/nanocrystalline coatings, Ultrason. Sonochem. 39 (2017) 39–46, <https://doi.org/10.1016/j.ulsonch.2017.04.011>.
- [8] S. Hong, Y. Wu, J. Zhang, Y. Zheng, Y. Qin, J. Lin, Ultrasonic cavitation erosion of high-velocity oxygen-fuel (HVOF) sprayed near-nanostructured WC–10Co–4Cr coating in NaCl solution, Ultrason. Sonochem. 26 (2015) 87–92, <https://doi.org/10.1016/j.ulsonch.2015.01.012>.
- [9] X. Ding, X. Cheng, X. Yu, C. Li, C. Yuan, Z. Ding, Structure and cavitation erosion behavior of HVOF sprayed multi-dimensional WC–10Co4Cr coating, Trans. Nonferrous Met. Soc. Chin. 28 (2018) 487–494, [https://doi.org/10.1016/S1003-6326\(18\)64681-3](https://doi.org/10.1016/S1003-6326(18)64681-3).
- [10] H. Zhang, Y. Gong, X. Chen, A. McDonald, H. Li, A comparative study of cavitation erosion resistance of several HVOF-sprayed coatings in deionized water and artificial seawater, J. Therm. Spray Technol. 28 (2019) 1060–1071, <https://doi.org/10.1007/s11666-019-00869-x>.
- [11] W. Deng, G. Hou, S. Li, J. Han, X. Zhao, X. Liu, Y. An, H. Zhou, J. Chen, A new methodology to prepare ceramic-organic composite coatings with good cavitation erosion resistance, Ultrason. Sonochem. 44 (2018) 115–119, <https://doi.org/10.1016/j.ulsonch.2018.02.018>.
- [12] W. Deng, X. Zhao, Y. Ren, E. Hao, J. Han, Y. An, H. Zhou, J. Chen, Influence of epoxy resin on the microstructure and cavitation erosion of as-sprayed 8YSZ coating, Ceram. Int. 45 (2019) 5693–5702, <https://doi.org/10.1016/j.ceramint.2018.12.034>.
- [13] Y. Tian, H. Zhang, X. Chen, A. McDonald, S. Wu, T. Xiao, H. Li, Effect of cavitation on corrosion behavior of HVOF-sprayed WC–10Co4Cr coating with post-sealing in artificial seawater, Surf. Coatings Technol. 397 (2020), 126012, <https://doi.org/10.1016/j.surfcoat.2020.126012>.
- [14] J. Zhang, M.O.W. Richardson, G.D. Wilcox, J. Min, X. Wang, Assessment of resistance of non-metallic coatings to silt abrasion and cavitation erosion in a rotating disk test rig, Wear. 194 (1996) 149–155, [https://doi.org/10.1016/0043-1648\(95\)06823-6](https://doi.org/10.1016/0043-1648(95)06823-6).
- [15] A. Yamaguchi, X. Wang, T. Kazama, Evaluation of erosion-resisting properties of plastics and metals using cavitating jet apparatus, SAE Int. (2002), <https://doi.org/10.4271/2002-01-1386>.
- [16] R. Guobys, Á. Rodríguez, L. Chernin, Cavitation erosion of glass fibre reinforced polymer composites with unidirectional layup, Compos. Part B Eng. 177 (2019), 107374, <https://doi.org/10.1016/j.compositesb.2019.107374>.
- [17] H. Bohm, S. Betz, A. Ball, The wear resistance of polymers, Tribol. Int. 23 (1990) 399–406, [https://doi.org/10.1016/0301-679X\(90\)90055-T](https://doi.org/10.1016/0301-679X(90)90055-T).
- [18] S. Hattori, T. Itoh, Cavitation erosion resistance of plastics, Wear. 271 (2011) 1103–1108, <https://doi.org/10.1016/j.wear.2011.05.012>.
- [19] T. Deplancke, O. Lame, J. Cavaillie, M. Fivel, M. Riondet, J. Franc, Outstanding cavitation erosion resistance of ultra high molecular weight polyethylene (UHMWPE) coatings, Wear. 328–329 (2015) 301–308, <https://doi.org/10.1016/j.wear.2015.01.077>.
- [20] P. Marlin, G.L. Chahine, Erosion and heating of polyurea under cavitating jets, Wear. 414–415 (2018) 262–274, <https://doi.org/10.1016/j.wear.2018.08.019>.
- [21] M. Narkis, J. Yacubowicz, A. Vaxman, A. Marmur, Electrically conductive composites prepared from polymer particles coated with metals by electroless deposition, Polym. Eng. Sci. 26 (1986) 139–143, <https://doi.org/10.1002/pen.760260205>.
- [22] Z. Jia, Y. Liu, Y. Wang, Y. Gong, P. Jin, X. Suo, H. Li, Flame spray fabrication of polyethylene-Cu composite coatings with enwrapped structures: a new route for constructing antifouling layers, Surf. Coatings Technol. 309 (2017) 872–879, <https://doi.org/10.1016/j.surfcoat.2016.10.071>.
- [23] T. Deplancke, O. Lame, F. Rousset, I. Aguilí, R. Seguela, G. Vigier, Diffusion versus cocrystallization of very long polymer chains at interfaces: experimental study of sintering of UHMWPE nascent powder, Macromolecules. 47 (2014) 197–207, <https://doi.org/10.1021/ma402012f>.
- [24] Y.H. Kim, R.P. Wool, A theory of healing at a polymer-polymer interface, Macromolecules. 16 (1983) 1115–1120, <https://doi.org/10.1021/ma00241a013>.
- [25] Y. Xue, T.A. Tervoort, S. Rastogi, J. Lemstra, Welding behavior of semicrystalline polymers. 2, Effect of cocrystallization on autoadhesion, Macromolecules. 33 (2000) 7084–7087, <https://doi.org/10.1021/ma000754y>.
- [26] C. Frederix, P. Beauchene, R. Seguela, J.M. Lefebvre, Kinetics of the non-isothermal fusion-welding of unlike ethylene copolymers over a wide crystallinity range, Polymer (Guildf). 54 (2013) 2755–2763, <https://doi.org/10.1016/j.polymer.2013.03.038>.
- [27] D. Jauffrès, O. Lame, G. Vigier, F. Doré, T. Douillard, Sintering mechanisms involved in high-velocity compaction of nascent semicrystalline polymer powders, Acta Mater. 57 (2009) 2550–2559, <https://doi.org/10.1016/j.actamat.2009.02.012>.
- [28] Y.A. Cengel, M.A. Boles, Thermodynamics: An Engineering Approach, 8th edition, 2015, <https://doi.org/10.1017/CBO9781107415324.004>.
- [29] ASTM G32-16, Standard test method for cavitation erosion using vibratory apparatus, ASTM Int. (2016), <https://doi.org/10.1520/G0032-10>.
- [30] D. Jauffrès, O. Lame, G. Vigier, F. Doré, Microstructural Origin of Physical and Mechanical Properties of Ultra High Molecular Weight Polyethylene Processed by High Velocity Compaction, 2007, <https://doi.org/10.1016/j.polymer.2007.07.058>.
- [31] K.Y. Chiu, F.T. Cheng, H.C. Man, Evolution of surface roughness of some metallic materials in cavitation erosion, Ultrasonics. 43 (2005) 713–716, <https://doi.org/10.1016/j.ultras.2005.03.009>.
- [32] S. Chi, J. Park, M. Shon, Study on cavitation erosion resistance and surface topologies of various coating materials used in shipbuilding industry, J. Ind. Eng. Chem. 26 (2015) 384–389, <https://doi.org/10.1016/j.jiec.2014.12.013>.
- [33] D. Jauffrès, O. Lame, G. Vigier, F. Doré, Microstructural origin of physical and mechanical properties of ultra high molecular weight polyethylene processed by high velocity compaction, Polymer 48 (2007) 6374–6383, <https://doi.org/10.1016/j.polymer.2007.07.058>.
- [34] J.-K. Choi, P. Marlin, G.L. Chahine, Experimental and numerical study of polyurea failure under cavitation, Proc. 5th Int. Symp. Mar. Propulsors, Espoo, Finland, June 11–15, 2017.